Analyst

Accepted Manuscript

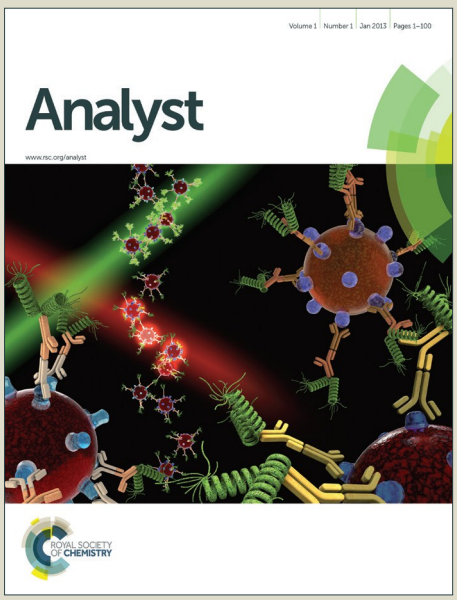

ROYAL SOCIETY OF CHEMISTRY

www.rsc.org/analyst

Raman microscopy at the subcellular level: study on early apoptosis in endothelial cells induced by Fas ligand and cycloheximide

K. Czamara[a,b], F. Petko[b], M. Baranska[a,b] A. Kaczor[a,b,*]

[a] Faculty of Chemistry, Jagiellonian University, Ingardena 3, 30-060 Krakow, Poland.

[b] Jagiellonian Centre for Experimental Therapeutics, Jagiellonian University, Bobrzynskiego 14, 30-348 Krakow, Poland.

* Corresponding author: kaczor@chemia.uj.eud.pl

Abstract

High spatially resolved Raman microscopy was applied to study the early apoptosis in endothelial cells and chemical and structural changes induced by this process. Application of cluster analysis enabled separation of signals due to various subcellular organelles and compartments such as nuclei, nucleoli, endoplasmic reticulum or cytoplasm and analysis of alterations locally at the subcellular level. Different stimuli, i.e. Fas ligand, a tumor necrosis factors, and cycloheximide, an inhibitor of eukaryotic protein biosynthesis, were applied to induce apoptotic mechanisms. Due to different mechanism of action, the changes observed in subcellular structures were different for FasL and cycloheximide. Although in both cases statistically significant decrease of the protein level was observed in all studied cellular structures, the increase of the nuclei acid content locally in apoptotic nuclei was considerably more pronounced upon Fas-induced apoptosis compared to cycloheximide one. Additionally, apoptosis invokes also a decrease of the proteins with the α-helix protein structure selectively for FasL in cytoplasm and endoplasmic reticulum.

Key words: Raman microscopy, endothelium, apoptosis, Fas ligand, cycloheximide

Introduction

Understanding of mechanisms and pathways of cellular processes requires insight into subcellular cell structures. Due to its label-free characteristic and the advantage of high spatial resolving power, Raman microscopy emerges as a great tool for characterization and visualization, even in 3D,[1] of various organelles.[2–4] Application of Raman microscopy to *in vitro* cellular models enables detection and localization of biochemical changes upon development of pathologies or investigating various cellular mechanisms or actions.[5–10]

Apoptosis, a programmed cell death is defined by morphological changes involving the ultrastructural alterations i.e. chromatin condensation and fragmentation, membrane blebbing, cytoskeletal disruption, cytoplasmic and nuclear shrinkage.[11,12] In mammalians, the decision of a cell to undergo apoptosis can be induced by a variety of regulatory stimuli and is considered to proceed in two major pathways.[13] The first one involves mitochondria as initiators in the intrinsic pathway provoking the release of cytochrome c into cytosol. After subsequent events, combined with the activation of executioner caspases, apoptosis leads to a cell death.[14] Contrarily to mitochondria-mediated apoptosis, the second pathway starts with binding of specific ligands, for example Fas ligand, to the death receptors on the cell membrane. Thus, the cascade of molecular actions, including proteolysis of caspases, is triggered.[15] Additionally, the endoplasmic reticulum also can induce apoptosis by upregulating the Ca^{2+} level or redox imbalance.[16]

Fas ligand (FasL) and cycloheximide (CHX) are examples of inducers sharing the ability to begin the apoptotic process.[17–21] In case of FasL-mediated programmed cell death, the killing signal in apoptosis is triggered after trimerization of the surface Fas molecules by binding of FasL. Fas, also termed Apo-1 or CD95, is the type I membrane protein and a representative of the death receptor subgroup of the tumor necrosis factor family.[22] The cell death mediated via Fas/FasL pathway plays an important role not only for maintaining the homeostasis of cells but also in the progress of different pathologies and diseases such as HIV and cancer.[20,23–25] CHX is an antibiotic, acquired from bacteria *Streptomyces griseus*, and was reported to act as an inhibitor of eukaryotic translation elongation of protein biosynthesis in cells.[17,26,27] CHX binds to the E-site of the large ribosomal subunit and blocks eEF2-mediated tRNA translocation, the process crucial in translation mRNA into proteins.[27,28] Overall, the action in apoptosis process of protein synthesis inhibitors is like a double-edged sword, it can both induce and inhibit apoptosis, so in other

words, it can lead to restraint of the continuous production of protective molecules and inhibition of death gene expression. The first effect seems to be more crucial for cell viability.[17–19] Moreover, CHX's impact on apoptosis is not obvious, it depends on the cell type, suggesting that pathways leading to apoptosis differ from one cell type to another. In hepatocytes, CHX induces overexpression of genes (i.e. c-myc) responsible for production of proteins significant in transducing the apoptotic signal.[17] On the other hand, it causes the increase of sphingosine level, a toxic product of the sphingomyelin cycle, that restrain protein kinase c and bcl-2 production, proteins involved in apoptosis inhibition.[17] Other studies indicate the activation of the caspase-3-like protease and decrease in mitochondrial membrane potential after CHX stimulation.[29] The same caspase-3 death machinery is activated in B lymphocytes,[19] whereas, in leucocytes CHX is recognized as an apoptotic pathway mediator with the cytotoxic effect on cells.[18]

Raman spectroscopy was applied so far to investigate apoptotic process within various types of cells after exposure to different stimuli i.e. cytotoxic drugs,[30–32] chemical agents[33] or harmful UV radiation.[34] However, there are no reports on apoptosis-mediated alterations induced via death receptors in endothelial cells studied with the help of Raman microscopy. The vast majority of papers is focused on studying the action of anticancer drugs and its chemotherapeutic response in anticancer therapy[30,32,35] or dedicated to classify and discriminate cells in apoptosis,[36–38] or to describe apoptotic process in details.[33,39–43] The programmed cell death studied by Raman spectroscopy reveals characteristic changes in band intensities due to alterations in biomolecules concentrations. In general, apoptosis is associated with the decrease in protein and DNA content manifested by the decrease, among others, of intensity of bands at 785 and 1007 cm^{-1}, assigned to ring breathing modes in the DNA and/or RNA bases and phenylalanine, respectively.[33,35,37,39] However, concentration of DNA is known to be dependent on a stage of the apoptosis, particularly, the increase of intensity of the band at 785 cm^{-1} is attributed to the early stages of the process.[36,40,42]

In this work, Raman microscopy was used to investigate alterations of the biochemical composition of endothelial cells with chemically induced apoptosis. Here, we focus on the early changes in programmed cell death as a result of FasL and CHX exposure. In particular, we aimed at determining the differences in the subcellular structures in cells, in which apoptosis was induced by different factors. Overall, Raman microscopy with its high resolving power enabled

characterization of subcellular changes in the endothelial cells upon apoptosis stimulated by FasL versus cycloheximide.

Experimental

Cells culture

To study *in vitro* the influence of apoptosis-inducing specimens on endothelium, the human endothelial cells EA.hy926 were selected as one of the best characterized immortalized endothelial cells.[44] Originally, EA.hy926 cells were created by fusing primary human umbilical vein cells (HUVECs) with a thioguanine-resistant clone of human lung carcinoma cell line A549.[45] The cells for Raman measurements were directly seeded onto calcium fluoride slides (CaF_2, 25 × 2 mm, Crystran LDT, UK) in the concentration of $2 \cdot 10^5$ cells/well. Cells were cultured in Dulbecco's Modified Eagle's Medium (DMEM, Gibco Life Technologies) including L-glutamine and supplemented with the 10% fetal bovine serum (FBS), 1% antibiotics (penicillin–streptomycin) and 2% HAT medium supplement. The cell cultures were maintained in a 37°C, 5% CO2/95% air cell culture incubator. After 24 hours incubation, when the confluence at the level of about 70% was obtained, cells were washed two times with phosphate buffered saline (PBS) and divided into two groups. The incubation times and doses of Fas ligand and cycloheximide are typical and commonly used for incubation of cells.[46,47] One group was exposed to 10 ng mL^{-1} human Fas ligand (FasL, Sigma) for 30 minutes (FasL group), and the second one was treated with cycloheximide (CHX, Sigma) in the concentration of 10 μg mL^{-1} for 3 hours (CHX group). As a control group, unstimulated EA.hy926 cells maintained in DMEM, were used. After stimulation cells were fixed with 4% glutaraldehyde for 4 minutes and stored in PBS buffer until data acquisition.

Raman measurements

WITec alpha 300 Confocal Raman Imaging system (WITec GmbH, Ulm, Germany) equipped with the UHTS 300 spectrograph (600 lines mm^{-1} grating) and a CCD detector (Andor, DU401A-BV-352) was used for Raman imaging. The air-cooled solid state laser with the excitation wavelength of 532 nm was used to excite the sample. Laser light was provided via a single mode

optical fiber (50 μm), and focused on to the sample by the 63× water immersive objective, (Zeiss, NA=1.0). Spectra were acquired with the 0.4 μm step in both x and y directions, 0.5 s integration time and the laser power at the sample of *ca.* 30 mW. At least 8 cells for each group (FasL, CHX, control) were measured.

Data analysis and processing

Data processing was performed using the WITec Project Plus software. All spectra were baseline corrected using autopolynomial of degree 2 and processed by a routine cosmic rays removal procedure. The subsequent application of cluster analysis (CA) (*k*-means method with the Manhattan distance) enabled to group spectra from the acquired datasets into classes reflecting the major organelles within cells. Average spectra of classes were used further for calculations of the integral intensity of various bands in the OPUS 7.0 program and only the following bands: 720, 785, 1007 cm^{-1} were presented as representative for biochemical alterations occurring after stimulation. Integral intensities of the well separated bands were calculated after spectra normalization in the range of 1500-400 cm^{-1} to minimize the water contribution to the intensity. The intensities were taken from the peak contour to the baseline. The analysis of variance was performed using a statistical model ANOVA with Tukey's test in the OriginPro 9.1 software. Analysis was provided to characterize quantitatively the differences in the biomolecules content in main cellular components in all pairwise comparisons for each group (FasL, CHX, control) and identify any difference between two means at the significance level of 0.05. The ImageJ processing program[48] was applied to calculate the nucleus, nucleoli and endoplasmic reticulum areas.

Results and discussion

The general features of endothelial cells after FasL and CHX stimulation

Due to its high resolving power, Raman microscopy provides the insight into biochemical composition and spatial distribution of bio-components at the subcellular level. The first step of this work was determination of the distribution of key components related to main organelles and cellular compartments. Fig. 1 shows reflected light microphotographs of the representative

control cells and cells treated with FasL and CHX. Raman distribution images of major cellular components (Fig. 1a-e) in the marked (Fig. 1A-C) areas of measurement were obtained based on the integration of characteristic marker bands. As presented on microphotographs, control endothelial EA.hy926 cells are spindle-shaped with capillary-like structures that are absent or reduced in number for cells after exposure to FasL and CHX agents (Fig. S1, Supplementary Material). That involution of the capillary network seems to be crucial hallmark of early apoptosis.[12,49]

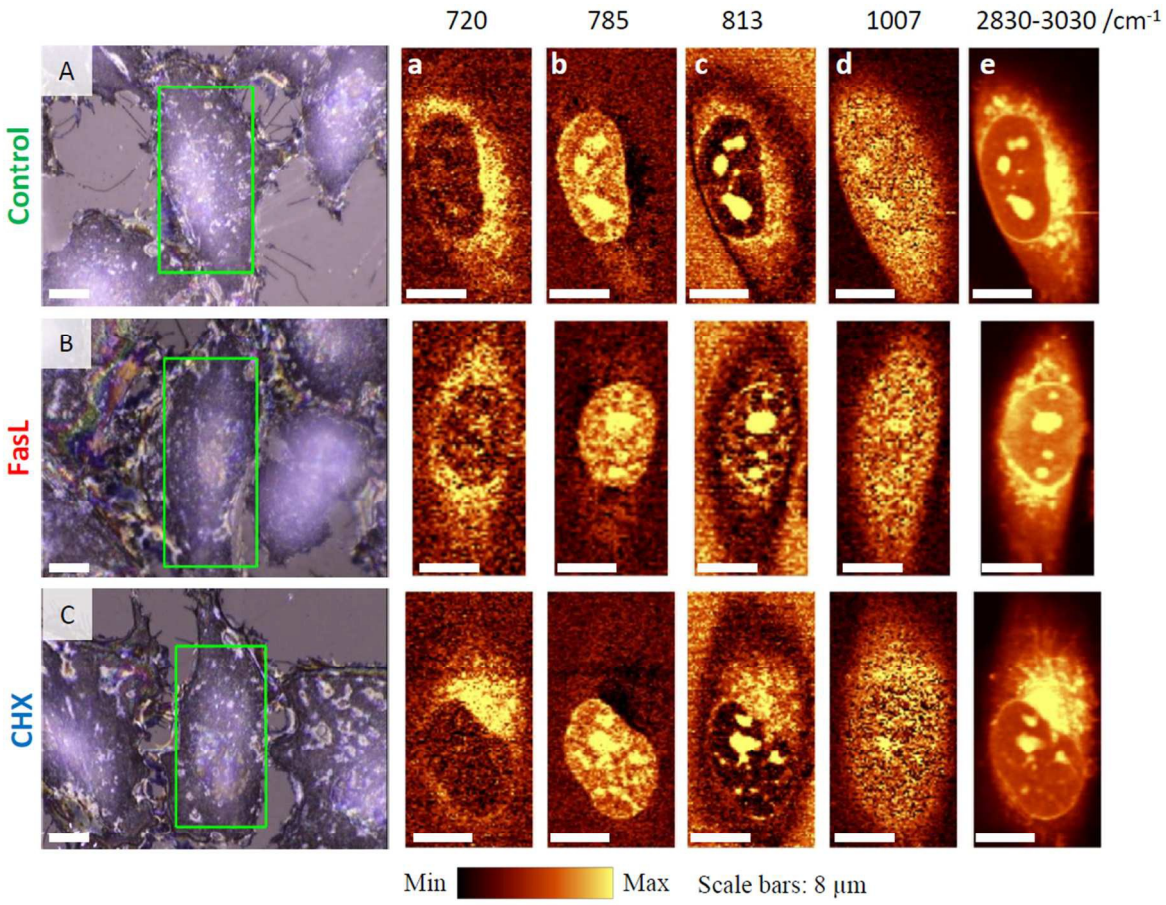

Figure 1. Representative visual and Raman images of control EA.hy926 cells and EA.hy926 cells stimulated with Fas ligand and cycloheximide. The reflected light microphotographs at 63× magnification (A-C) with marked imaged areas and Raman distribution images (a-e) of representative cells from the control, FasL and CHX groups. Raman distribution images were obtained by integration of characteristic bands for phospholipids (720 cm^{-1}), DNA&RNA (785 cm^{-1}), RNA (813 cm^{-1}), proteins (1007 cm^{-1}) and all biomolecules in the range of 2830-3030 cm^{-1}.

The Raman images (1a-e) were obtained by integration of key marker bands assigned to the $N^+(CH_3)_3$ symmetric stretching vibrations of choline moiety at 720 cm^{-1} (column 1a),[50] the ring breathing modes in the DNA&RNA bases at 785 cm^{-1} (column 1b),[51] the symmetric O−P−O (in C'_5-O-P-O-C'_3 phosphodiester) stretching vibrations in RNA at 813 cm^{-1} (column 1c),[51,52] the symmetric breathing mode of phenylalanine at 1007 cm^{-1} (column 1d)[53] and the C-H stretching vibrations in the range of 2830-3030 cm^{-1} (column 1e). Due to the high resolving power of Raman microscopy, obtained Raman images can be related to subcellular components and compartments. Thus, the first column (1a) shows areas of high concentration of phospholipids, especially phosphatidylcholine, being one of the major constituents of cellular membranes, i.e. related mostly to endoplasmic reticulum, mainly in the vicinity of the cell nuclei. Two subsequent columns (1b and 1c) exhibit the distribution of both DNA and RNA in the areas corresponding to nuclei and nucleoli. The distribution images obtained by integration of the RNA band at 813 cm^{-1} are the additional confirmation of the localization of endoplasmic reticulum as they show ribosomal RNA in ribosomes attached to its structure. The images in two last columns (1d and 1e) refer to distribution of proteins and all organic biomolecules, respectively, and enable to define the borders of the cell body and main sub-cellular components simultaneously. Overall, obtained Raman images for FasL and CHX treated cells do not reveal any significant visible changes in distribution of biomolecules in comparison to the control.

Chemical characteristics of early apoptosis in endothelial cells

To characterize chemical alterations upon FasL and CHX stimulations in a detailed way, we used cluster analysis (CA, *k*-means with the Manhattan distance) for imaging results of the same representative cells as in Fig. 1. Presented CA images (Fig. 2) demonstrate a high compliance with the distribution images (Fig. 1). However, the subtle differences in the Raman signatures of various classes are clearly observed (Fig. 2B).

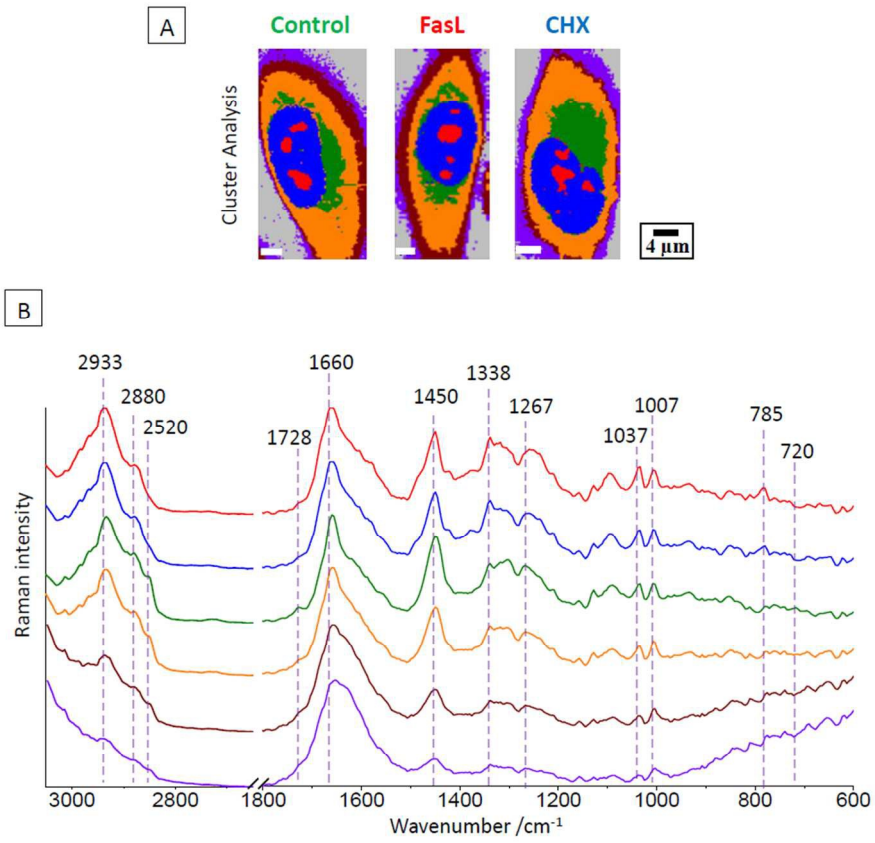

Figure 2. Cluster analysis images of control EA.hy926 cell, FasL- and cycloheximide-stimulated EA.hy926 cells with average Raman spectra of each class. Cluster images of representative control (green) and stimulated with FasL (red) and CHX (blue) cells (6 classes: red – nucleoli; blue class – nucleus; green – endoplasmic reticulum; orange – cytoplasm, brown – cell membrane; violet – adhesion proteins) and the Raman spectra of respective clusters for a single control cell. All spectra were maximally extended in both x and y ranges.

The advantage of CA approach is that the spectral information from each class is averaged enabling to determine the subcellular response to chemical stimulation. Here, four classes, identified as nucleoli (red), nucleus (blue), endoplasmic reticulum (green) and cytoplasm containing small organelles e.g. mitochondria (orange), were investigated. Two remaining classes related with the cell membrane (brown) and adhesion proteins (violet) were omitted in this analysis as their signal was of low-intensity and contained contribution from the surroundings.

The average spectra of mentioned four well defined subcellular compartments, averaged over at least 8 cells, are presented in Fig. 3.

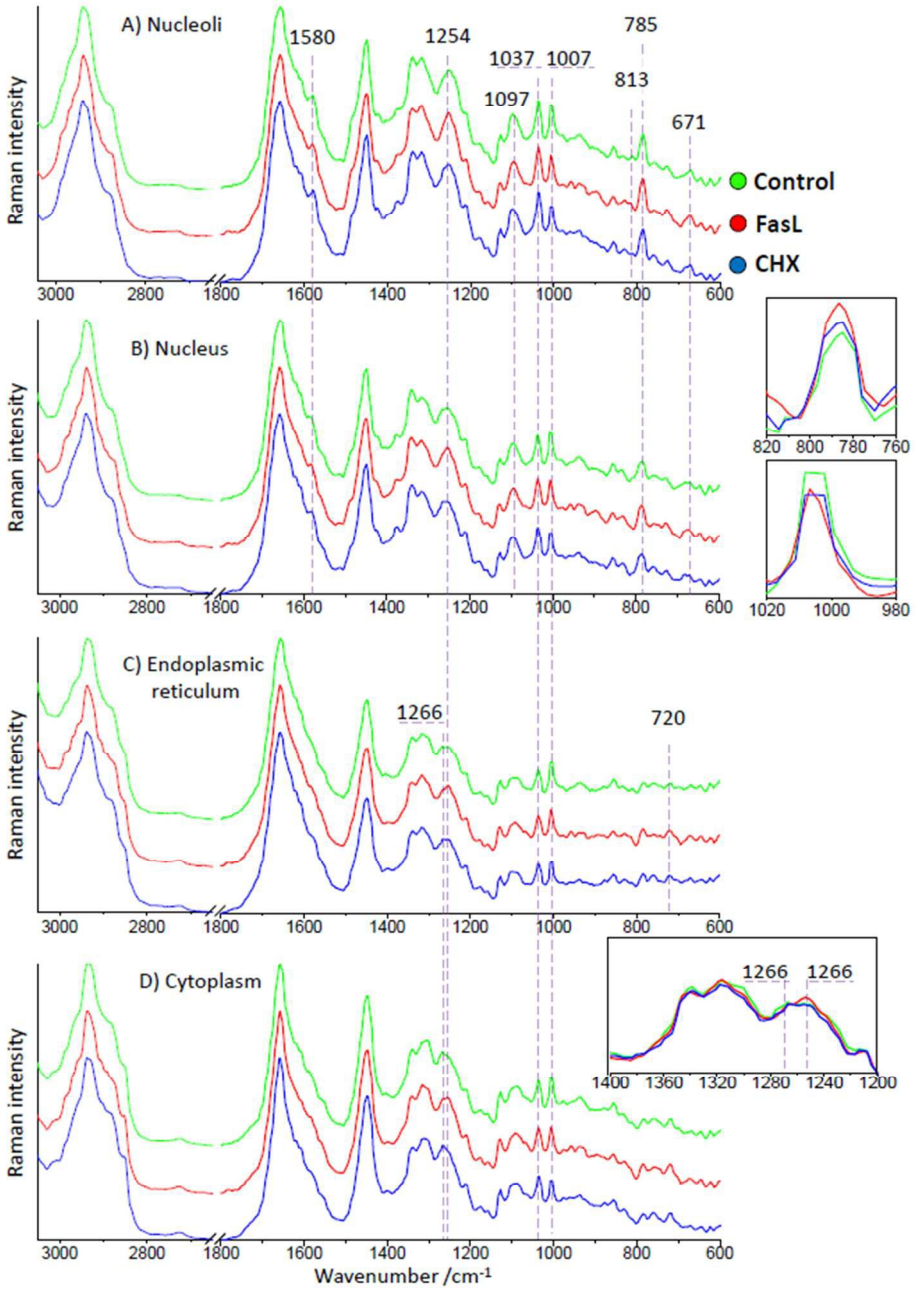

Figure 3. Cluster analysis of control EA.hy926 cells and EA.hy926 cells stimulated with Fas ligand and cycloheximide. The average Raman spectra of nucleoli (A), nucleus (B), endoplasmic reticulum (C) and cytoplasm (D) for control, FasL- and cycloheximide-stimulated cells denoted with green, red and blue, respectively. All spectra were maximally extended in both x and y ranges. The inserts show changes in intensity of bands at 785 and 1007 cm^{-1} for the nucleus class and in the amide III range for the cytoplasm class.

The spectral profile of nucleoli and nuclei (Fig. 2 sections A and B, respectively) is marked mostly by the presence of bands at 671, 785, 1097 and 1580 cm^{-1}, originating from the nucleic acid vibrations, and characteristic both for DNA and RNA, and the signal at 813 cm^{-1}, distinctive for RNA molecules.[51,52] The intensity of these bands show the increase for cells exposed to FasL and (only slightly) to CHX compared to the control ones what is clearly seen for the signal at 785 cm^{-1}. Alterations in the nucleotide concentration are associated with the elevated chromatin condensation and are characteristic for the early apoptosis.[42,54] After nuclear condensation in the late stage of apoptosis, DNA is cut into short fragments that are thrown out from the cell leaving an empty shell of the cellular membrane what is naturally manifested as a decrease of the DNA bands' intensity.[32] Nevertheless, it is not excluded that this effect can overlap with the additional effect of the intensity decrease, as chain scission may result in relatively lower intensity of the DNA signal compared to the signal of a longer (uncut) chain. Although at this level we cannot verify if this effect is a cause of the decrease of the DNA signal, the overall increase in the intensity of the DNA bands observed after stimulation demonstrates that the observed changes are, indeed, signs of the early stage of apoptosis.[36,40,42] However, these are not only changes observed for apoptoticaly-altered cells. Raman bands with maxima at 1656 cm^{-1} (amide I), 1254 cm^{-1} (amide III) and two characteristic signals at 1037 and 1007 cm^{-1}, assigned to the symmetric ring breathing mode of phenylalanine, are typical Raman features of proteins.[53] The range of amide I and III is also characteristic for the bands originating from lipids, i.e. the stretching vibration of the C=C bond at 1660 cm^{-1} and CH_2 twisting mode at 1300 cm^{-1}, thus, the band at 1007 cm^{-1} was chosen to study changes in proteins content. In all mentioned cell components a decrease in intensity of the phenylalanine band at 1007 cm^{-1} after FasL and CHX stimulation was noticed. This change, slightly more pronounced for CHX stimulation compared to the FasL one, is the most characteristic feature of early apoptosis, observed in this study. The most distinctive band at 720 cm^{-1} in the spectra of endoplasmic reticulum (Fig. 3 section C) originates from the stretching vibrations in choline/ethanolamine moieties of phospholipids.[50] Moreover, in the spectra of endoplasmic reticulum and cytoplasm of cells exposed to FasL in the range of amide III other alterations are observed. Here, the maximum of the amide III band is red-shifted to 1254 cm^{-1}, in contrast to the spectra from the control and CHX groups, where maximum of this signal is seen at 1266 cm^{-1}. The amide III range is sensitive to the protein secondary structure changes and the observed shift (from 1254 cm-1 to 1266 $cm^{-}1$) can be identified as the structural

transition from the α-helix to β-sheet, through unordered structure.[55,56] In many diseases, for example related to amyloid formation (type II diabetes, Alzheimer's or Parkinson's), the structural α-β transition of proteins is a common feature.[57] The maximum of amide III band at 1254 cm^{-1} indicates the decrease in the α-helix content in the endoplasmic reticulum and cytoplasm of the cells from the FasL group. These observations can be associated with of caspases release and its action, in which this cysteine proteases catalyze the hydrolysis of peptide bond causing secondary structure alterations and subsequent protein degradation. It also suggests the different apoptotic mechanism depending on the used agent. Overall, significant changes are revealed in endothelial cells upon early apoptosis, manifested by the elevated level of DNA in nuclei and nucleoli (only slightly for CHX) with the simultaneous decrease in proteins in the whole cell.

Subcellular versus cellular changes upon apoptosis progression – the semi-quantitative approach

The changes in biomolecules content upon a stimuli can be identified using principal component Analysis (PCA, Fig. S2 and Fig. S3, Supplementary Material) and semi-quantitively measured as the integral intensity of the marker bands in normalized Raman spectra and analyzed by ANOVA statistical tests. The analysis performed by PCA and ANOVA shows the same trends in changes in the chemical composition observed after stimulation of cells. It is worth noticing that PCA separation of groups was considerably better in case if individual organelles (Fig. S2) and not the whole cells (Fig. S3) were used for the analysis. For ANOVA, the integral intensity of the marker bands at 1007, 785 and 720 cm^{-1} assigned to proteins, DNA/RNA and phospholipids, respectively, were calculated for each organelle. The results are presented in Fig. 4.

Following the discussion about changes in the average CA spectra (*vide supra*), it is seen in Fig. 4 that the level of proteins in the early apoptotic cells is significantly lower compared to the control cells. The explanation of the decrease of protein concentration lies in the mechanism of induced apoptosis. In both cases, FasL and CHX trigger the molecular pathways involving the production and activation of various caspases, a family of cysteine proteases,[13] that in turn lead to protein degradation.[24] Evident differences in the DNA/RNA content within nucleus and nucleoli

in the cells in the early stage of apoptosis are also observed, of the opposite direction compared to the protein content. In both organelles, the elevated level of nucleic acids is observed. Nevertheless, only in cells exposed to FasL, this change is statistically significant, meaning that the effect of death receptor-stimulated apoptosis is stronger than mediated by a protein translation inhibitor, such as CHX. Also the concentration of phospholipids slightly (but statistically insignificantly) increased in the endoplasmic reticulum upon FasL stimulation.

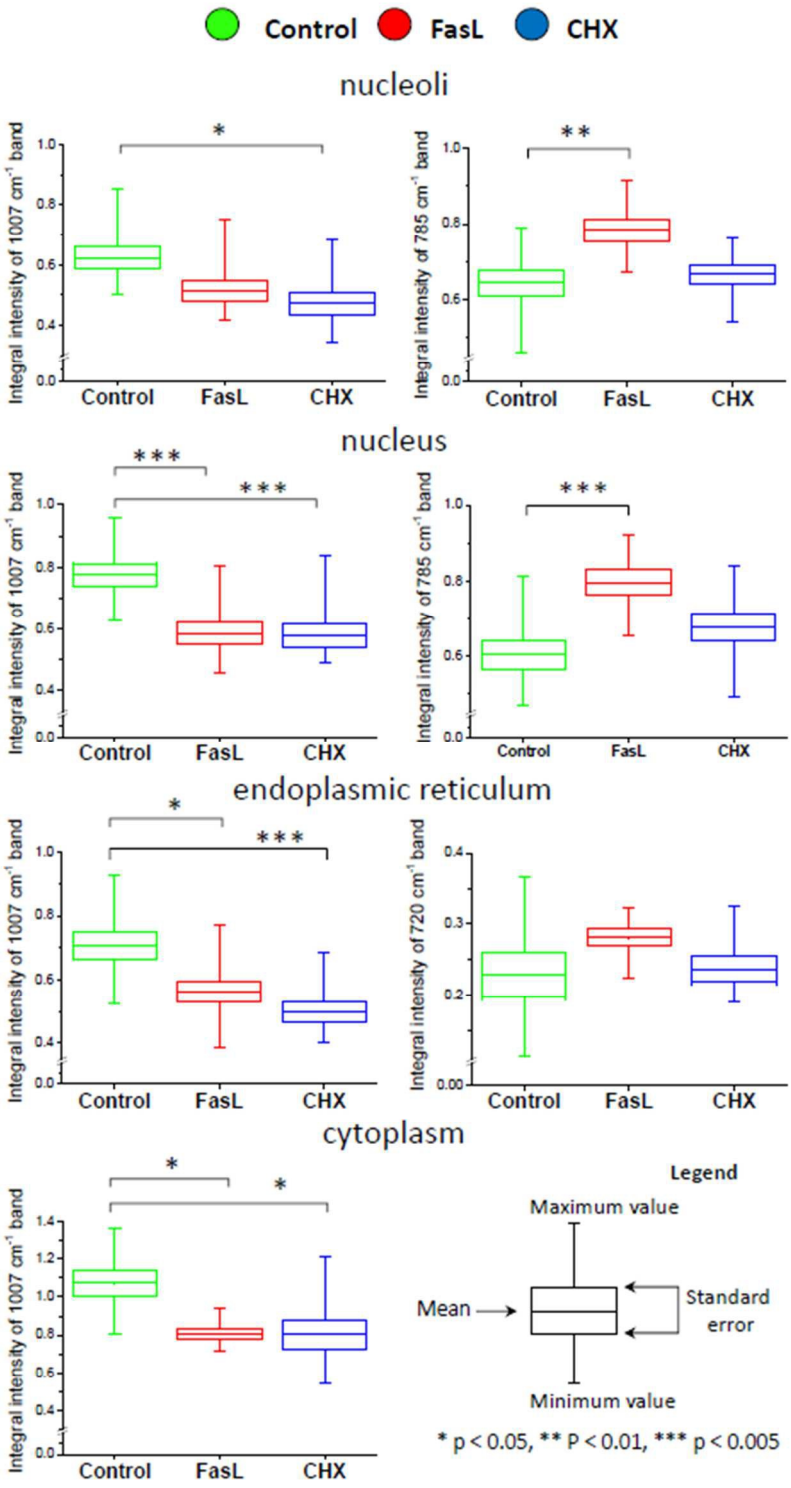

Figure 4. Chemical changes in subcellular components upon early apoptosis. Integral intensity of marker bands at 785, 1007 and 720 cm^{-1} for nucleus, nucleolus, endoplasmic reticulum and cytoplasm for control cells, FasL- and CHX cell stimulation showing significant alterations in the concentration of DNA, and proteins within main cellular components.

The same approach as for subcellular organelles, was applied to investigate biomolecules content in the entire endothelial cells. Thus, the overall changes in endothelial cells upon early apoptosis were determined. The average Raman spectra of cells (A) and calculated integral intensity for the most characteristic bands (B) are presented in Fig. 5.

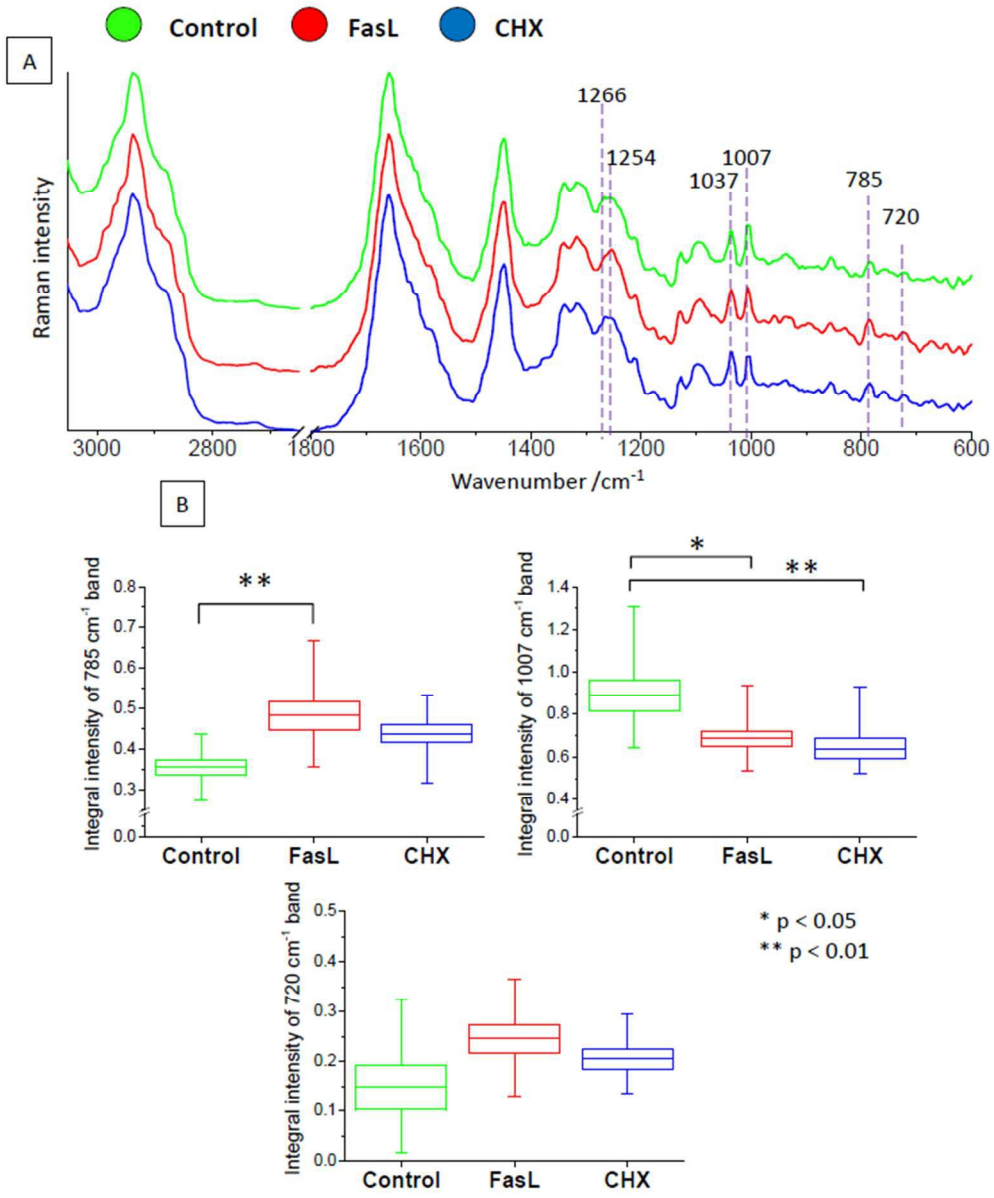

Figure 5. Chemical changes in EA.hy926 cells upon early apoptosis. The Raman spectra (A) averaged over entire cells and integral intensity of marker bands at 785, 1007 and 720 cm^{-1} after FasL and CHX stimulations compared to the control (B).

As expected, alterations of cellular components, observed for subcellular structures, are also reflected in the average spectra of the whole cell. The increased DNA content, statistically significant for FasL stimulation, and the reversed effect for the protein concentration after induced apoptosis is maintained. However, the changes are not so clear because the information is blurred over the entire cell. Additionally, information about localization of chemical changes in particular organelles is lost. Locating the chemical alterations upon a stimuli is crucial for understanding the mechanism of cellular events involved in the development of endothelial dysfunction and in the future to design the adequate drug therapy. The possibility of molecular biochemical assignments at the subcellular level is an advantage of high spatially resolved Raman imaging.

Along with the quantitative measurement of biomolecules concentration, the area of Raman images covered by nucleus, nucleoli and endoplasmic reticulum were calculated (Fig. 6).

The investigation was performed on Raman images classified as nucleoli, nucleus and endoplasmic reticulum as obtained from CA. The results show that alterations in DNA/RNA content and the nucleus area were significant (p-values, with 5% level of decision using the Tukey test in ANOVA, equal 0.054 and 0.011 for FasL and CHX, respectively) and that the increased level of nucleotides correlates with the increased area of nucleus calculated as percent of the area of whole cell covered by nucleus. In this study nuclei slightly enlarge, probably due to condensation of chromatin along the perimeter of the nucleus,[12] with simultaneous cell shrinkage after FasL and CHX treatment. This observation is not typical for apoptosis, in which cell nuclei overall decrease,[58,59] but it can be a feature of its early stage. For nucleoli and reticulum, no statistically significant changes were noticed.

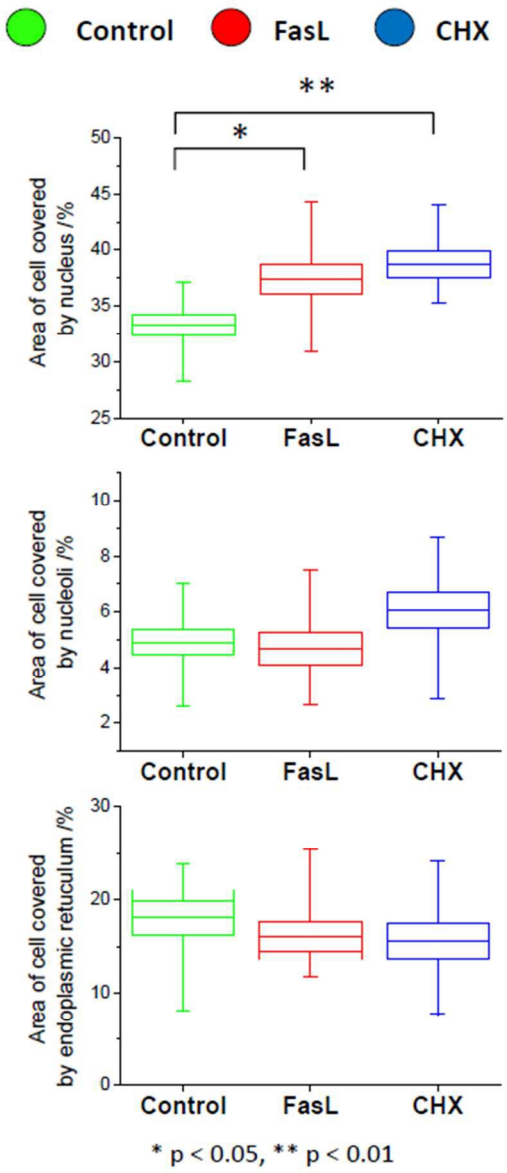

Figure 6. Size statistics of cell components upon FasL and CHX exposure compared to the control. The calculated area of nucleus, nucleoli and endoplasmic reticulum refers to the total cell surface.

Conclusions

Understanding of mechanisms of cell apoptosis is of prime importance, due to the fact that defects in the apoptotic pathways leads to development of cancer. Fas ligand is one of the apoptotic factors that has frequently a changed expression in human cancer cells.[60] FasL induces

the apoptotic process *via* linking to its death receptor on the cell membrane and triggering the cascade of various molecular actions.[17–21] Caspases, activated during FasL-induced apoptotic pathways, cleave in turn key structural proteins.[61] Cycloheximide, another apoptosis inducer, acts differently, *via* binding to the ribosomal subunit and blocking protein synthesis, more specifically tRNA translocation.[27,28] To verify if and how these different apoptotic pathways influence the cells and their chemical composition, we applied Raman imaging and chemometric tools. We concentrated on the early apoptotic process and localized chemical alterations specifically in the subcellular structures and compartments such as nuclei, endoplasmic reticulum and cytoplasm. The analysis of variance (ANOVA with Tukey's test) of the normalized average spectra of subcellular structures for apoptotic and control cells demonstrated that upon both FasL and CXH stimulation a statistically significant decrease in the protein (a marker band at 1007 cm^{-1}) content is observed in the nucleus, endoplasmic reticulum and cytoplasm. It shows that a decrease of the protein level is independent on the apoptotic trigger (at least for these two factors used here) and is not spatially localized (occurs for all cell compartments). This effect agrees with the fact that upon both apoptotic pathways, mechanisms leading to degradation of proteins (caspases activation for both factors) and, additionally, a direct inhibition of their synthesis (tRNA translocation blockage for CHX) are induced. Contrarily, only for FasL a statistically significant increase of the nucleic acid (a marker band at 785 cm^{-1}), limited to nuclei and nucleoli area, is shown. This effect is due to elevated chromatin condensation and was described previously as a process characteristic for the early apoptosis.[42,54] The increase of nucleic acids' signal is considerably lower (and not statistically significant) in apoptotic cells upon CHX influence most probably due to the fact that CHX is an "external" agent acting directly on protein synthesis. Nevertheless, both for FasL and CHX slight augmentation of the area covered by the cell nuclei is observed upon stimulation compared to the control. All these changes of the chemical composition in the subcellular structures are reflected in the global cell spectra, where both the decrease of protein and the increase in the nuclei acids level were also observed. Apart for the chemical changes, apoptosis invokes also structural alterations of the proteins both in endoplasmic reticulum and cytoplasm of cells, but only selectively for cells exposed to FasL and not CHX, compared to the control. Overall, Raman microscopy enabled characterization of the chemical and structural alterations in subcellular structures of the endothelial cells upon development of early apoptosis in a semi-quantitative manner demonstrating also that the

influence of different mechanisms of apoptosis on chemical composition in subcellular structures can be studied.

Acknowledgements

The project was supported by National Science Centre (DEC-2013/08/A/ST4/00308) and the European Union from the resources of the European Regional Development Fund under the Innovative Economy Programme (grant coordinated by JCET-UJ, POIG.01.01.02-00-069/09). KCz thanks the Krakow Scientific Marian Smoluchowski Consortium "Matter - Energy - Future" for financial support.

References

1. K. Majzner, A. Kaczor, N. Kachamakova-Trojanowska, A. Fedorowicz, S. Chlopicki, and M. Baranska, *Analyst*, 2013, **138**, 603–10.

2. C. Matthäus, T. Chernenko, J. A. Newmark, C. M. Warner, and M. Diem, *Biophys. J.*, 2007, **93**, 668–673.

3. A. F. Palonpon, M. Sodeoka, and K. Fujita, *Curr. Opin. Chem. Biol.*, 2013, **17**, 708–715.

4. Z. Farhane, F. Bonnier, A. Casey, A. Maguire, L. O'Neill, and H. J. Byrne, *Analyst*, 2015, **140**, 5908–5919.

5. G. Clemens, J. R. Hands, K. M. Dorling, and M. J. Baker, *Analyst*, 2014, **139**, 4411–4444.

6. A. S. Stender, K. Marchuk, C. Liu, S. Sander, M. W. Meyer, E. A. Smith, B. Neupane, G. Wang, J. Li, J. X. Cheng, B. Huang, and N. Fang, *Chem. Rev.*, 2013, **113**, 2469–527.

7. M. Baranska, A. Kaczor, K. Malek, A. Jaworska, K. Majzner, E. Staniszewska-Slezak, M. Z. Pacia, G. Zajac, J. Dybas, and E. Wiercigroch, *Pharmacol. Reports*, 2015, **67**, 736–743.

8. C. Matthäus, S. Boydston-White, M. Miljković, M. Romeo, and M. Diem, *Appl. Spectrosc.*, 2006, **60**, 1–8.

9. A. D. Meade, C. Clarke, F. Draux, G. D. Sockalingum, M. Manfait, F. M. Lyng, and H. J. Byrne, *Anal. Bioanal. Chem.*, 2010, **396**, 1781–1791.

10. C. Krafft, T. Knetschke, R. H. W. Funk, and R. Salzer, *Anal. Chem.*, 2006, **78**, 4424–4429.

11. M. Bhatia, *Am. J. Physiol. Gastrointest. Liver Physiol.*, 2004, **286**, G189–G196.

12. G. Häcker, *Cell Tissue Res.*, 2000, **301**, 5–17.

13. M. O. Hengartner, *Nature*, 2000, **407**, 770–6.

14. C. Wang and R. J. Youle, *Annu. Rev. Genet.*, 2009, **43**, 95–118.

15. K. Schulze-Osthoff, D. Ferrari, M. Los, S. Wesselborg, and M. E. Peter, *Eur. J. Biochem.*, 1998, **254**, 439–459.

16. R. V Rao, H. M. Ellerby, and D. E. Bredesen, *Cell Death Differ.*, 2004, **11**, 372–380.

17. A. V. Alessenko, Boikov, G. N. Filippova, A. V. Khrenov, A. S. Loginov, and E. D. Makarieva, *FEBS Lett.*, 1997, **416**, 113–116.

18. D. Baskić, S. Popović, P. Ristić, and N. N. Arsenijević, *Cell Biol. Int.*, 2006, **30**, 924–932.

19. C. Lemaire, K. Andréau, V. Souvannavong, and A. Adam, *Biochem. Pharmacol.*, 1999, **58**, 85–93.

20. P. Waring and A. Müllbacher, *Immunol. Cell Biol.*, 1999, **77**, 312–317.

21. S. Nagata, *Cell*, 1997, **88**, 355–365.

22. H. O. Lee and T. A. Ferguson, *Cytokine Growth Factor Rev.*, 2003, **14**, 325–335.

23. D. H. Dockrell, *Clin. Microbiol. Infect.*, 2003, **9**, 766–779.

24. M. Ehrenschwender and H. Wajant, *Adv. Exp. Med. Biol.*, 2009, **647**, 64–93.

25. B. Poonia, C. D. Pauza, and M. S. Salvato, *Retrovirology*, 2009, **6**, 91–99.

26. D. Kerridge, *J. Gen. Microbiol.*, 1958, **19**, 497–506.

27. T. Schneider-Poetsch, J. Ju, D. E. Eyler, Y. Dang, S. Bhat, W. C. Merrick, R. Green, B. Shen, and J. O. Liu, *Nat. Chem. Biol.*, 2010, **6**, 209–217.

28. T. G. Obrig, W. J. Culp, W. L. McKeehan, and B. Hardesty, *J. Biol. Chem.*, 1971, **246**, 174–181.

29. W. M. Blom, H. J. G. M. De Bont, I. Meijerman, G. J. Mulder, and J. F. Nagelkerke, *Biochem. Pharmacol.*, 1999, **58**, 1891–1898.

30. H. Huang, H. Shi, S. Feng, W. Chen, Y. Yu, D. Lin, and R. Chen, *Anal. Methods*, 2013, **5**, 260–266.

31. K. le Roux, L. C. Prinsloo, and D. Meyer, *Appl. Phys. Lett.*, 2014, **105**, 123702–123706.

32. T. J. Moritz, D. S. Taylor, D. M. Krol, J. Fritch, and J. W. Chan, 2010, **1**, 1138–1147.

33. B. Li, M.-Q. Lu, Q.-Z. Wang, G.-Y. Shi, W. Liao, and S.-S. Huang, *Chinese J. Anal. Chem.*, 2015, **43**, 643–650.

34. E. Lipiec, K. R. Bambery, P. Heraud, W. M. Kwiatek, D. McNaughton, M. J. Tobin, C. Vogel, and B. R. Wood, *Analyst*, 2014, **139**, 4200–4209.

35. H. Yao, Z. Tao, M. Ai, L. Peng, G. Wang, B. He, and Y. Q. Li, *Vib. Spectrosc.*, 2009, **50**, 193–197.

36. E. Brauchle, S. Thude, S. Y. Brucker, and K. Schenke-Layland, *Sci. Rep.*, 2014, **4**, 4698–4707.

37. Y. H. Ong, M. Lim, and Q. Liu, *Opt. Express*, 2012, **20**, 25041–25055.

38. J. Panza and J. Maier, in *Imaging, Manipulation, and Analysis of Biomolecules, Cells, and Tissues V*, eds. D. L. Farkas, D. V. Nicolau, and R. C. Leif, Proceedings of SPIE, San Francisco, 2007, vol. 6441, pp. 6441081–64410812.

39. S. Verrier, I. Notingher, J. M. Polak, and L. L. Hench, *Biopolymers*, 2004, **74**, 157–162.

40. X. Jiang, Z. Jiang, T. Xu, S. Su, Y. Zhong, F. Peng, Y. Su, and Y. He, *Anal. Chem.*, 2013, **85**, 2809–2816.

41. A. Pliss, A. N. Kuzmin, A. V Kachynski, and P. N. Prasad, *Proc. Natl. Acad. Sci. U. S. A.*, 2010, **107**, 12771–12776.

42. A. Zoladek, F. C. Pascut, P. Patel, and I. Notingher, *J. Raman Spectrosc.*, 2011, **42**, 251–258.

43. N. Uzunbajakava, A. Lenferink, Y. Kraan, E. Volokhina, G. Vrensen, J. Greve, and C. Otto, *Biophys. J.*, 2003, **84**, 3968–3981.

44. D. Bouïs, G. A. P. Hospers, C. Meijer, G. Molema, and N. H. Mulder, *Angiogenesis*, 2001, **4**, 91–102.

45. C. J. Edgell, C. C. McDonald, and J. B. Graham, *Proc. Natl. Acad. Sci. U. S. A.*, 1983, **80**, 3734–7.

46. A. Y. Zhang, F. Yi, G. Zhang, E. Gulbins, and P. L. Li, *Hypertension*, 2006, **47**, 74–80.

47. A. Toulmay and W. A. Prinz, *J. Cell Biol.*, 2013, **202**, 35–44.

48. C. A. Schneider, W. S. Rasband, and K. W. Eliceiri, *Nat. Methods*, 2012, **9**, 671–675.

49. M. J. Pollman, L. Naumovski, and G. H. Gibbons, *J. Cell. Physiol.*, 1999, **178**, 359–70.

50. K. Czamara, K. Majzner, M. Pilarczyk, K. Kochan, A. Kaczor, and M. Baranska, *J. Raman Spectrosc.*, 2015, **46**, 4–20.

51. Z. Movasaghi, S. Rehman, and I. U. Rehman, *Appl. Spectrosc. Rev.*, 2007, **42**, 493–541.

52. A. Ghita, F. C. Pascut, M. Mather, V. Sottile, and I. Notingher, *Anal. Chem.*, 2012, **84**, 3155–3162.

53. A. Rygula, K. Majzner, K. M. Marzec, A. Kaczor, M. Pilarczyk, and M. Baranska, *J. Raman Spectrosc.*, 2013, **44**, 1061–1076.

54. D. Zhang, Y. Feng, Q. Zhang, X. Su, X. Lu, S. Liu, and L. Zhong, *Spectrochim. Acta Part A Mol. Biomol. Spectrosc.*, 2015, **141**, 216–222.

55. N. C. Maiti, M. M. Apetri, M. G. Zagorski, P. R. Carey, and V. E. Anderson, *J. Am. Chem. Soc.*, 2004, **126**, 2399–2408.

56. Z. Chi, X. G. Chen, J. S. Holtz, and S. A. Asher, *Biochemistry*, 1998, **37**, 2854–2864.

57. F. Chiti and C. M. Dobson, *Annu. Rev. Biochem.*, 2006, **75**, 333–366.

58. M. Rogalinska, *Cell. Mol. Biol. Lett.*, 2002, **7**, 995–1018.

59. V. L. Johnson, S. C. Ko, T. H. Holmstrom, J. E. Eriksson, and S. C. Chow, *J. Cell Sci.*, 2000, **113**, 2941–2953.

60. M. E. Peter, P. Legembre, and B. C. Barnhart, *Biochim. Biophys. Acta - Rev. Cancer*, 2005, **1755**, 25–36.

61. G. M. Cohen, *Biochem. J.*, 1997, **326**, 1–16.